RC pile–soil interaction analysis using a 3D-finite element method with fibre theory-based beam elements

Takeshi Maki[1,*,†], Koichi Maekawa[2] and Hiroshi Mutsuyoshi[1]

[1]*Department of Civil and Environmental Engineering, Saitama University, 255 Shimo-Okubo, Sakura-ku, Saitama 338-8570, Japan*
[2]*Department of Civil Engineering, The University of Tokyo, 7-3-1 Hongo, Bunkyo-ku, Tokyo 113-8656, Japan*

SUMMARY

To evaluate the overall response of a structural system including its foundation and surrounding soil, an equivalent finite element model with reduced degrees of freedom using fibre theory-based beam element was proposed. The proposed model was based on investigations of the subgrade soil reaction of a single layer model, and was verified for the cyclic behaviour of a laterally loaded single RC pile in terms of the load–displacement relationship, pile deformation, and soil pressures on the pile surface. Also investigated was the effect of the interfacial element between pile and soil on the behaviour of the laterally loaded pile.

KEY WORDS: RC pile; subgrade soil reaction; 3D-FEM analysis; fibre model; beam element; interface between pile and soil

1. INTRODUCTION

In the 1995 Hyogo-ken Nanbu earthquake, many reinforced concrete (RC) structures, especially expressway and railway structures, suffered serious damage. In contrast, the pile foundations that supported the superstructures suffered relatively little damage, except that the foundations were exposed to the lateral flow of the surrounding soil. Most of the superstructures were retrofitted after the earthquake. However, non-strengthened members, such as footings and piles, might be damaged during the next earthquake. Therefore, it is important to precisely evaluate the seismic performance of a structure overall including the superstructure, foundation, and surrounding soil.

From this perspective, response analysis using the finite element (FE) method in the time domain, in which seismic motion is input to the engineering base layer, is an advanced technique for evaluating the overall response of structural systems. This method automatically and explicitly considers the interactions between RC members or between a pile and the surrounding soil. The ability to obtain detailed damage information about the constitutive materials is another advantage of this method. Such a method is already a standard technique for evaluating the safety of important civil engineering structures such as nuclear power facilities [1]. Its use has also been prescribed in the JSCE standard specifications for concrete structures (seismic performance verifications), which was revised in 2002 [2].

* Correspondence to: Takeshi Maki, Department of Civil and Environmental Engineering, Saitama University, 255 Shimo-Okubo, Sakura-ku, Saitama 338-8570, Japan.
† E-mail: maki@post.saitama-u.ac.jp

Thus far, numerous studies and investigations have been conducted on the seismic behaviour of pile foundations based on the horizontal subgrade reaction (*p–y* curve) method for calculating the restoring force of pile foundations. The current design methods of pile foundations are based on the theory of the beam on Winkler springs (BWS) model, in which the experimentally obtained *p–y* curves are used for characterizing the springs [3–6]. This method, however, does not take soil continua into account and might not be appropriate for detailed analysis. In contrast, many investigations of pile foundation behaviours using FE analysis have also been performed [7–9]. Wakai *et al.* [10] investigated the effect of the types of non-linear constitutive laws of soil on the lateral resistance of piles, and Zhang *et al.* [11] applied the t_{ij} model to the soil model to simulate the lateral behaviour of pile foundation. In both studies, the chief interest was given to the non-linear soil models, and the 3-D solid elements were used as a pile model.

A full 3-D analysis is desirable when considering the three-dimensional effect of pile–soil interaction. However, due to high computational costs, the modeling of all the structural members using solid elements might not be feasible, especially for structures such as large tanks that are supported on a large number of piles. Hence, to analyze the seismic response of an entire system of such structures including the effect of the soil, it is desirable to develop an equivalent FE model, with reduced degrees of freedom (DOF), which can achieve reasonable analytical results within reasonable computational costs. The principal objective of this paper is to propose such an equivalent model based on the grouping of material and element models in 3-D FE analysis. Therefore, with regard to the future application to overall structural response analysis with input seismic waves at the engineering base layer, the DOF-reduced model discussed in this paper stands intermediate between the existing studies on the simple *p–y* model and on the detailed full 3-D FE model.

Figure 1 compares the lateral load and displacement relationships at the head of single pile. These relationships were obtained from existing experiments and 3-D FE analyses [12]. In both of the models, joint elements were provided between pile and soil in order to remove the tensile stress. The hysteresis curve obtained from the analysis using 3-D solid elements for pile modeling agreed well with the experimental result, while the result obtained by pile modeling with beam elements had relatively low accuracy. These results revealed that the appropriate grouping of the models is highly important.

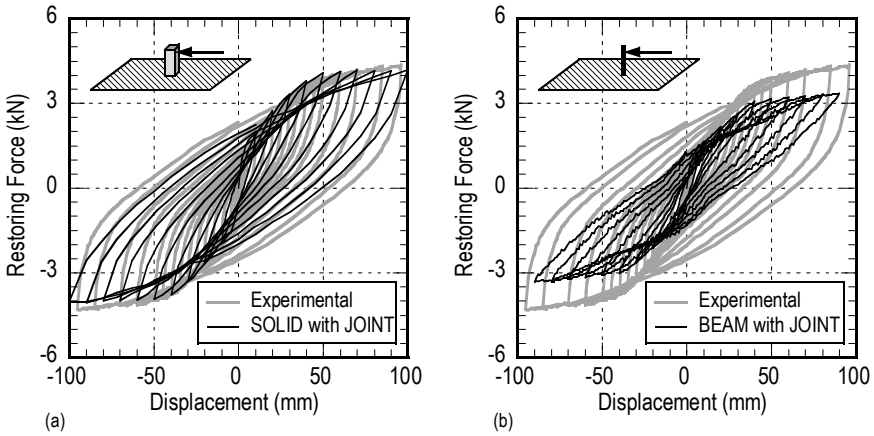

Figure 1. Load and displacement relationships of RC pile–soil system calculated by: (a) full-3D solid element model; and (b) 3D-beam element model.

This paper discusses the application of a fibre theory-based beam element model to RC pile–soil interaction analysis. Prior to the FE analysis of the pile–soil system, subgrade soil reactions were investigated based on single-layer FE models. The proposed DOF-reduced model was verified using the results of cyclic loading tests of a single RC pile in sand soil [12–15]. The effect of localized interaction at the pile–soil interface on the response behaviour of RC pile–soil systems is also discussed.

2. CYCLIC LOADING TEST OF SINGLE RC PILES

Figure 2(a) shows the experimental setup. A single RC pile specimen was fastened to a rigid steel box, and the box was filled with dry sand having a uniform grain diameter. The properties of the sand [16] are listed in Table I. Lateral reversed cyclic displacements were applied at the pile head through a loading actuator. Strain gauges and earth pressure cells attached to the surface of the pile were used to measure pile deformations and subgrade soil reactions, respectively. The pile specimen was securely fastened to the bottom of the steel box to prevent rotation, whereas the pile head was allowed to rotate freely. Overall soil deformation was confined by the rigid soil box during loading. Although the conditions of the experiment were as close as possible to the actual conditions of the piles, some specific conditions were chosen to provide clear boundary conditions so that the results could be used in subsequent analyses.

The experimental parameters consisted of the cross-sectional shape and longitudinal reinforcement ratio of the RC pile, and the stiffness of the soil. The soil stiffness was controlled by changing the relative density of the soil. Additional cases using two elastic piles were included in the experimental program in order to verify the variations in the subgrade soil reactions on the surface of the pile. All of the experimental cases are summarized in Table II.

Figure 2(b) shows the cross sections of the specimens. All of the specimens had an equal width of 100 mm in the loading direction. Deformed bars having a diameter of 6 or 10 mm were used as longitudinal reinforcements. Deformed bars having a diameter of 3.2 mm were arranged with 100mm spacing as lateral reinforcements. The elastic steel pile specimen had a hollow rectangular cross section with an initial bending stiffness (*EI*) equal to that of the RC specimens.

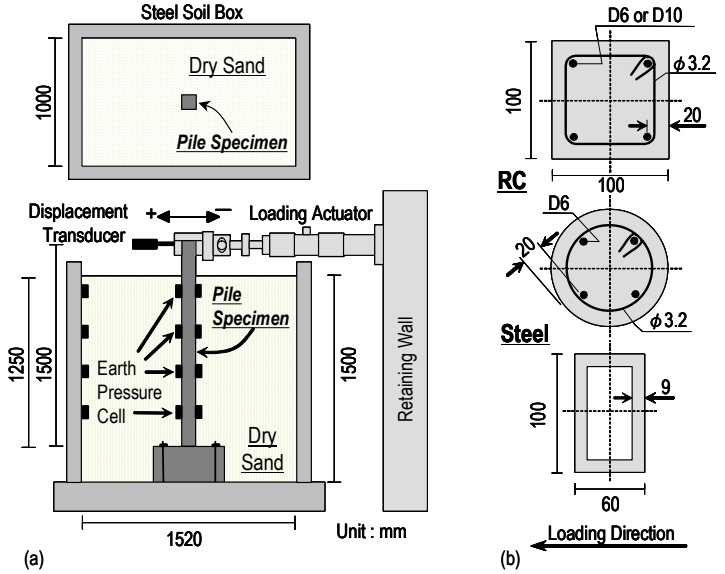

Figure 2. (a) Experimental loading system; and (b) cross sections of test specimens.

Table I. Properties of Gifu sand.

Specific Gravity	G_s	2.643
Maximum Diameter	D_{max} (mm)	0.84
60% Diameter	D_{60} (mm)	0.35
30% Diameter	D_{30} (mm)	0.31
10% Diameter	D_{10} (mm)	0.22
Uniformity Coefficient	U_c	1.59
Maximum Void Ratio	e_{max}	1.126
Minimum Void Ratio	e_{min}	0.717

Table II. Experimental variables of test cases.

No.	Case	Type	Section Shape	f_c' (N/mm^2)	Long. Reinf.	Soil Condition	Soil D_r (%)	K_R (x10^{-3})
1	RCX-L	RC	Square	43.0	4-ϕ10	Loose	55.53	0.747
2	RCR-L	RC	Square	45.3	4-ϕ6	Loose	55.53	0.404
3	RCR-D	RC	Square	42.3	4-ϕ6	Dense	67.27	0.342
4	RCC-D	RC	Circle	44.3	4-ϕ6	Dense	71.28	0.203
5	STR-L	Steel	Hollow	------	------	Loose	55.53	1.497
6	STR-D	Steel	Hollow	------	------	Dense	73.49	1.212

The relative density of the soil was controlled by consolidating the soil layer at a thickness of every 30 cm using a concrete block dropped onto the ground surface. The resulting relative density in each case is listed in Table II. The initial horizontal earth pressures were measured in all cases and the initial earth pressure coefficient K_h/v, which is defined as the ratio of the horizontal to the vertical pressures, ranged from 0.5 to 0.7 in the cases with loose soil, and from 2.3 to 4.0 in the cases with dense soil. The relative pile-to-soil stiffness was calculated for each case using the above soil conditions and Equation (1) proposed by Poulos [17]:

$$K_R = \frac{E_p I_p}{E_s L^4} \tag{1}$$

where E_p is the elastic modulus of the pile, I_p is the moment of inertia of the pile, E_s is the initial elastic modulus of the soil, and L is the embedded length of the pile. Here, E_s was calculated by

$$E_s = 2(1+\nu)G_0 \tag{2}$$

where G_0 is the initial shear modulus and ν is Poisson's ratio. The assumed Poisson's ratio here was equal to 0.3. The initial shear modulus (G_0) was calculated by the following equation:

$$G_0 = 630\frac{(2.17-e)^2}{1+e}\sigma_c^{0.321} \tag{3}$$

where G_0 is in kgf/cm^2, e is the void ratio, and σ_c is the initial confining pressure in kgf/cm^2 [16].

The calculated K_R values are listed in Table II.

Focusing on the force transfer mechanism between the single pile and the soil, the results of these experiments were used to verify the proposed equivalent model. Therefore, when applying the proposed model to actual structures, it is desirable to examine the measuring error and accuracy of the soil parameters as well as the adequacy of the soil constitutive model applied to the actual soil model. Furthermore, the analytical model should be carefully verified in the future for three-dimensional behaviour such as group pile effect.

3. SUBGRADE SOIL REACTION ON PILE SURFACE

3.1. Sectional force and subgrade soil reaction

When a pile foundation is exposed to seismic motion at the engineering base layer, the piles are subjected not only to the inertial force of the superstructure but also to the soil pressures induced by soil deformation, as shown in Figure 3(a). Concerning the governing differential equation shown in the figure, it is desirable to precisely estimate the subgrade soil reaction, $p(z)$. Therefore, in order to calculate the accurate response of the pile, the analytical model should be utilized for appropriately evaluating the stress transmission between the pile and the soil. As already shown in Figure 1, the DOF-reduced model consisting of beam and joint elements underestimates the lateral load, while a full 3-D solid element model provides better accuracy. In the case of a laterally loaded single pile, the subgrade soil reaction, vertically distributed from the ground surface level to the maximum moment location, governs the lateral load, as illustrated in Figure 3(b). In this section, the influence of FE modeling on the resultant subgrade soil reaction is explained in detail [18].

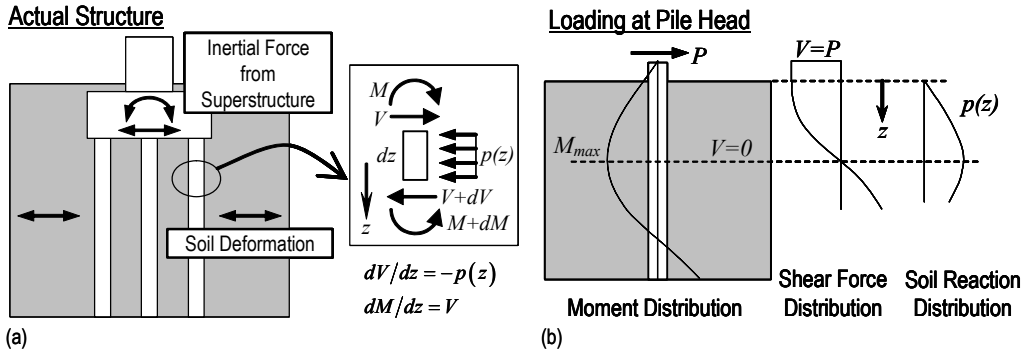

Figure 3. (a) Governing equations under earthquake; and (b) sectional force distributions of pile subjected to inertial lateral load.

3.2. Analytical models and parameters

Three-dimensional FEM code COM3 [19, 20] developed at The University of Tokyo was used in the analytical study. The basic FE models are shown in Figure 4. Targeting the loading test of a single RC pile explained in the previous section, subgrade soil reactions were investigated based on a single-layer model. Soil was modeled as 20-node solid elements in the single-layer model. For the modeling of a concrete pile, a 3-node fibre theory-based beam element (FB) and a 20-node solid element (SL) were compared. As far as the flexural behaviour of the pile is concerned, it is better to keep the thickness of each soil layer small in the FE model for the pile–soil interaction analysis. Hence, for both of the basic models SL and FB, the thickness of the soil layer was taken as 10cm, equal to the diameter of the pile. Monotonic lateral displacement in the X direction was applied to all nodes of the pile elements.

The analytical parameters are listed in Table III. In addition to the element model of the pile, the effect of the presence of a joint element between the pile and the soil, the mesh division width around the pile, and the Gauss integration order were also examined. Here, the interface element includes the contact and separation between the pile and the soil. 16-node 2-D joint elements were applied to SL, and 6-node 1-D joint elements were provided in FB, as shown in Figure 5.

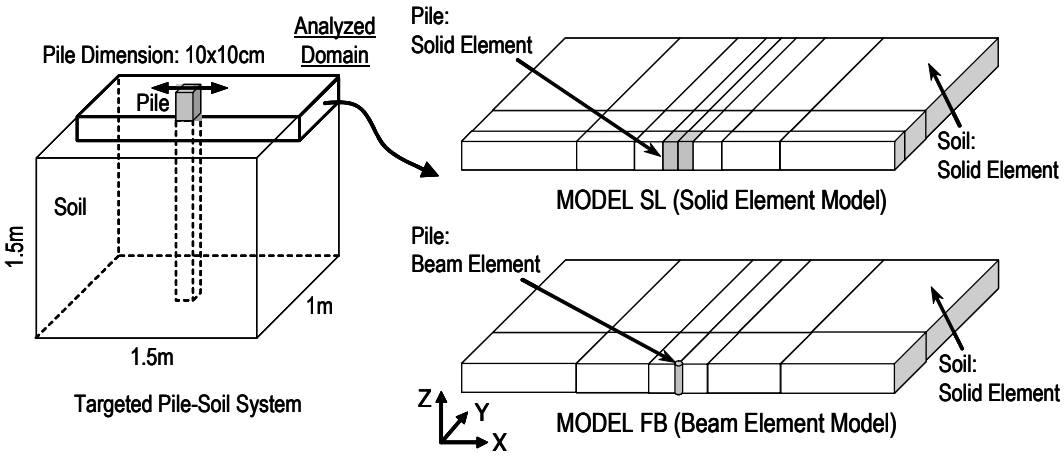

Figure 4. Basic single-layer model.

Table III. Analytical parameters and cases.

Element Type	Case	Interface	Mesh Division	Gauss Integration
Solid	SL	no	------	2
	SL-J	yes	------	2
Beam	FB	no	coarse	2
	FB-J	yes	coarse	2
	FB-fine	no	fine	2
	FB-J-fine	yes	fine	2
	FB-g5	no	coarse	5
	FB-J-g5	yes	coarse	5

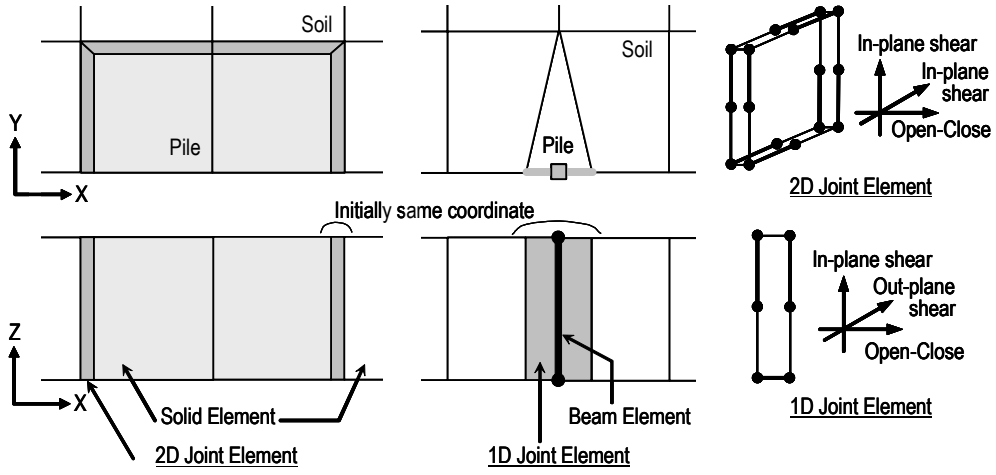

Figure 5. Profiles of joint element.

Model SL-J was similar to the model that gave a reasonable accuracy for the load–displacement curve shown in Figure 1(a). The 1-D joint element was produced by reducing the DOF of the Mindlin plate element, and it linked three nodes in the beam element and the soil solid element. Each node in the joint element had three translational and three rotational DOF. However, in this analysis, the latter was ignored and all rotational components in the element stiffness matrix were null. In other words, the flexural moment induced in the beam element was not transmitted to the soil element. Therefore, only the normal, in-plane shear and out-of-plane shear stresses based on the three translational DOF were transmitted between the beam and the solid elements. Both the 1-D and 2-D joint elements had high rigidity in compression, while small values were given for the tensile and shear rigidities. The influence of the mesh division width was examined using the fine mesh models shown in Figure 6. The width of the mesh division perpendicular to the loading direction in these models was smaller than in the basic models. A Gauss integration order of 2 was used for solid elements (reduced Gauss integration) in the basic models; however, an integration order of 5 was adopted in FB-g5 in order to examine the effects of localized stress transmission.

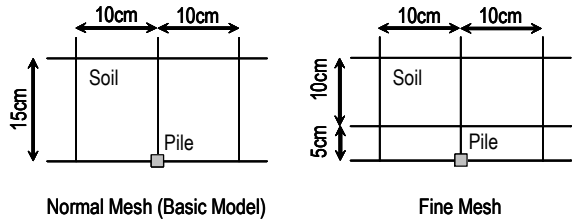

Figure 6. Mesh division width.

The Osaki model [21] was used as a soil material model, which defines the relationship between the second deviatoric invariant stress J_2 and strain J_2 as shown in

$$\frac{J_2'}{M} = \frac{J_2}{2G_0 M}\left\{1+\left(\frac{G_0}{100S_u}-1\right)\left|\frac{J_2}{S_u M}\right|^B\right\} \tag{4}$$

where G_0 is the initial shear modulus, S_u is the shear strength at 1% shear strain calculated by the following Equation (5), B is the material parameter (1.6 for sand and 1.4 for clay), and M is the loading parameter (1.0 when loading, and 2.0 when unloading or reloading):

$$S_u = c\cdot\cos\phi + \sigma_c\cdot\sin\phi \tag{5}$$

where σ_c is the initial confining pressure. c and ϕ are the cohesion and the internal friction angle, which are assumed to have constant values of 0.001 [N/mm^2] and 27.5 [deg], respectively [16]. The initial shear modulus (G_0) and the shear strength at 1% shear strain (S_u) were determined from the experimental conditions.

This model was already verified up to the 1% shear strain level based on stratified soil response [21], and the tangential modulus beyond the 1% shear strain was assumed to be a constant equal to that at the 1% shear strain. The principal tensile stress is allowed to occur, and the average (volumetric) component is assumed to be linear elastic, in which the volumetric elasticity is calculated from the initial shear modulus and Poisson's ratio (a constant value of 0.3 is assumed) based on the elasticity theory. In this material model, the effect of confinement (average stress state) on the shear behaviour was ignored.

3.3. Analytical results

Figure 7 shows the relationships between the lateral load and the displacement for all of the models. The lateral load is the sum of the reactions at all of the loading nodes, and the lateral displacement is expressed as a dimensionless value normalized by the pile diameter (=100 mm). The lateral load in FB was half that in SL and was close to that in SL-J. Furthermore, a remarkable decrease in the lateral load could be observed in FB-J compared with SL-J and FB due to the elimination of tensile stress in the rear of the pile body.

The influence of the mesh division width around the pile was barely seen in the model without a joint element, while it was significant in the model having a joint element. Since the soil elements in front of the pile were subjected to a line load when the pile was modeled by a beam element, the localized plasticity increased in the soil element in FB-J-fine, which resulted in a ceiling for the lateral load.

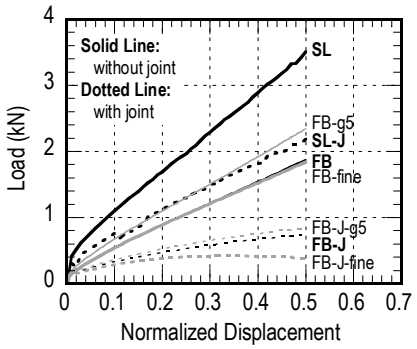

Figure 7. Load–displacement relationships.

A slightly higher lateral load was 1 observed in the model with 5-order Gauss integration, even for the same mesh division. This was because the Gauss point co-ordinate approached that of the pile element both in FB-g5 and FB-J-g5 so that the localized stresses at the Gauss points near the pile were sensitively reflected on the subgrade reaction rather than in the basic model. The results in FB-g5, as shown in Figure 7, were very close to that of SL-J. If the result of SL-J was regarded as the basis of evaluation, FB, FB-fine, and FB-g5 could give reasonable accuracies in terms of the *p–y* relationship.

3.4. Decomposed subgrade reaction around pile

The total subgrade reaction was decomposed into three types of reactions on the front, rear, and side surfaces of the pile by integrating the soil stresses at the Gauss points around the pile. Figure 8(a) is a schematic diagram of subgrade reaction decomposition in both the SL- and FB-type models. Examples of the stress integration results for SL and FB-J are shown in Figure 8(b). The proposed stress integrating scheme was applied in the following discussions on the subgrade reaction distribution around the pile.

Figure 9(a) shows the decomposed reactions of the piles in SL-J and FB. The total subgrade reactions in these two models were almost equal, as shown in Figure 7. However, the profiles of the decomposed reactions were different. In SL-J, the rear surface reaction was very low due to the tensile stress removal while the front surface reaction was high. In contrast, similar values of reactions could be observed on the front and rear surfaces in FB. Considering that SL-J was the closest model to the actual pile condition among all the examined models, a similar total reaction to SL-J could be obtained in FB by allowing tensile stress to occur in the soil elements, although the front surface reaction was underestimated due to the use of beam elements. Figure 9(b) shows

similar results that were obtained by FB and FB-fine, which gave an equal total reaction. However, the front and rear surface reactions in FB-fine were lower than those in FB, resulting in differences in the side reactions in these two models. Figure 9(c) shows the results for FB and FB-g5. The differences in the total subgrade reactions in these models (see Figure 7) originated from the excess increase in tensile force at the rear surface in FB-g5; the softening of the front surface reaction in FB-g5 was due to the localized plasticity of the soil around the pile. These decomposed reactions at the front and rear surfaces were not realistic even though the total subgrade reaction was close to that in SL-J. Figure 10 shows 1 the normal stress distributions in the soil at the front surfaces in SL-J, FB, and FB-fine. The stress distribution in FB was close to that in SL-J rather than that in FB-fine. Therefore, if beam elements are used for pile models, a realistic soil stress state could be obtained by using a coarse mesh division (about three times as large as the pile dimension, as in FB).

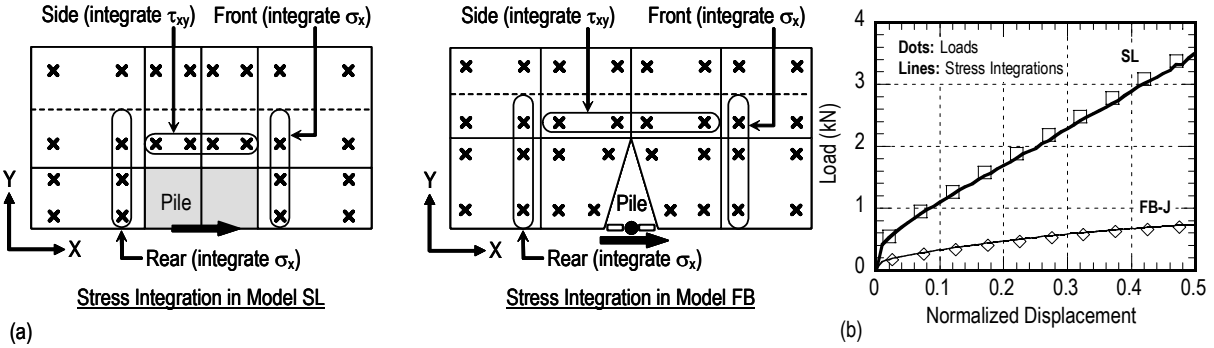

Figure 8. Decomposition of subgrade reactions: (a) stress integration concept; and (b) its verifications.

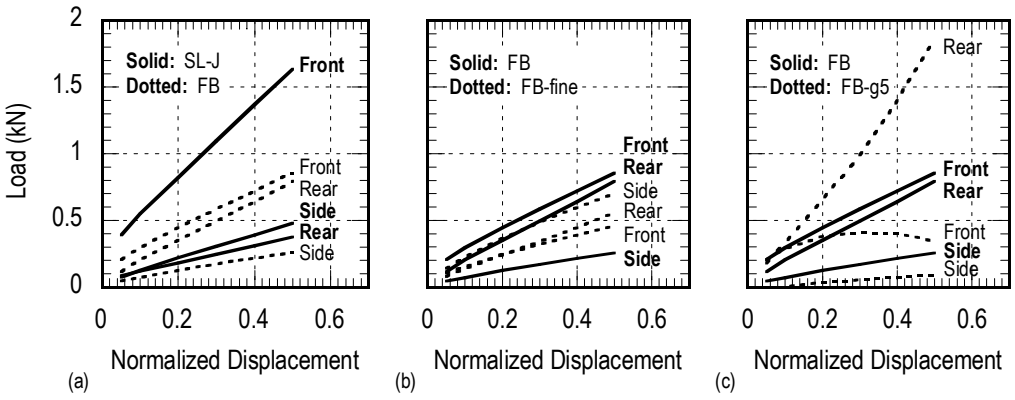

Figure 9. Comparisons between subgrade reaction shares in: (a) SL-J and FB; (b) FB and FB-fine; and (c) FB and FB-g5.

3.5. Summary

The influence of the pile model on subgrade soil reactions was discussed using a single-layer FE model. When a pile was modeled using a beam element, the decomposed front surface reaction was underestimated. However, when the principal tensile stress was allowed to occur in the soil material model and no joint element was provided between the pile and the soil, the total subgrade reaction was almost equal to that observed in the solid element model for the pile accompanied with joint elements. It is important to keep in mind the possibility of underestimating the total subgrade soil reaction when simultaneously using beam and joint elements. Moreover, the appropriate stress

distribution in the surrounding soil was obtained by using a relatively coarse mesh division around the pile. Therefore, from the viewpoint of the *p–y* relationship, an equivalent analysis using a beam element as a pile model could be performed based on the following analytical conditions:

— no joint element between pile and soil is provided;
— principal tensile stress is allowed to occur in the soil;
— relatively coarse mesh division around pile is recommended (about three times pile diameter seems appropriate);
— low order of Gauss integration scheme in soil elements is recommended (to avoid stress localization).

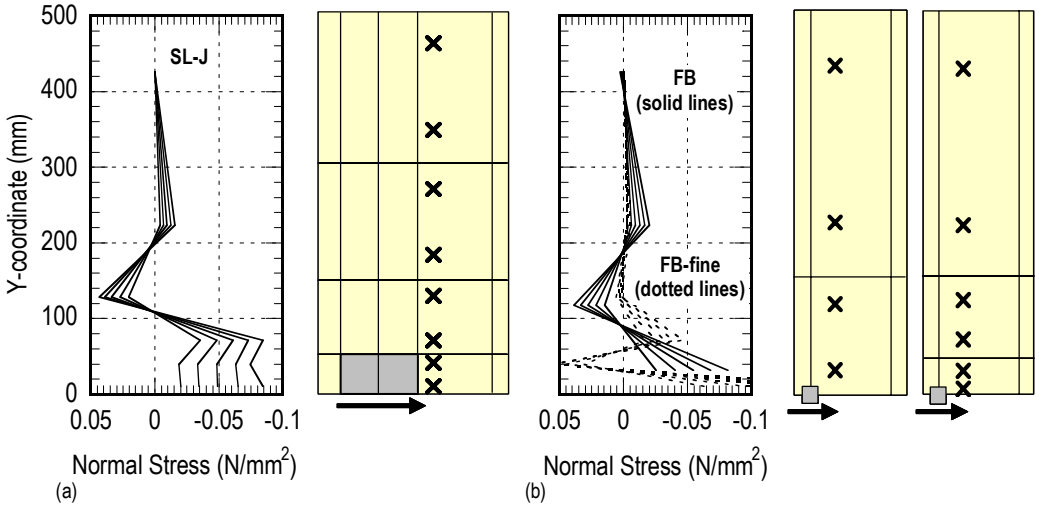

Figure 10. Normal stress distributions in: (a) model SL-J; and (b) model FB and FB-fine.

4. PILE–SOIL INTERACTION ANALYSIS

The cyclic behaviour of a laterally loaded single RC pile in sand soil was simulated by using the proposed DOF-reduced FE model. The analytical results were fully compared with the experimental results and the proposed equivalent model was verified. The effect of interfacial characteristics on the response of the pile–soil system was also investigated.

4.1. Analytical model and constitutive laws of reinforced concrete and soil

Figure 11(a) shows the FE mesh used for loading test simulations of the pile–soil system. The pile specimen was modeled using 3-node RC beam elements based on a fibre model [20], and no joint interface elements were provided between pile and soil. In the RC beam element, the axial force and two-directional flexural moments were calculated using the averaged axial strain and two-directional curvatures. In the calculation, the cross section of the element was divided into minute cells (fibres), as shown in Figure 11(b), in relation to the longitudinal reinforcement arrangement. The uniaxial stress–strain relationships of the concrete and the reinforcement [20], illustrated in Figure 12, were applied to each cell. These constitutive laws were obtained by modifying the existing three-dimensional constitutive laws for reinforced concrete [19]. Additionally, a zoning technique [22] was applied for the cross section, as shown in Figure 11(b). The RC zone represents an effective area of tension stiffening of the longitudinal reinforcement. The tension stiffening parameter (c) in the tensile stress–strain curve of concrete for the RC zone was a constant value of 0.4, while it was

dependent on the element size and the fracture energy for the plain concrete zone (PL). The confining effect of lateral reinforcements on the uniaxial stress–strain relationship of concrete was completely ignored in this analysis. The shear formulation of the element was assumed to be linear elastic.

The same constitutive law of the soil shown in Figure 12(c) was applied as in the previous section. In order to consider the vertically distributed shear parameters, the shear stiffness and strength of each layer were calculated by Equations (3) and (5), respectively [16]. As described previously, the material model did not include the confining effect on the shear behaviour and the plasticity in volumetric deformation such as dilatation and consolidation, as well as the effect of pore water on the mechanical behaviour of soil materials. In the future, detailed investigations on the effects of such characteristics of soil on the structural responses obtained by the proposed model are needed.

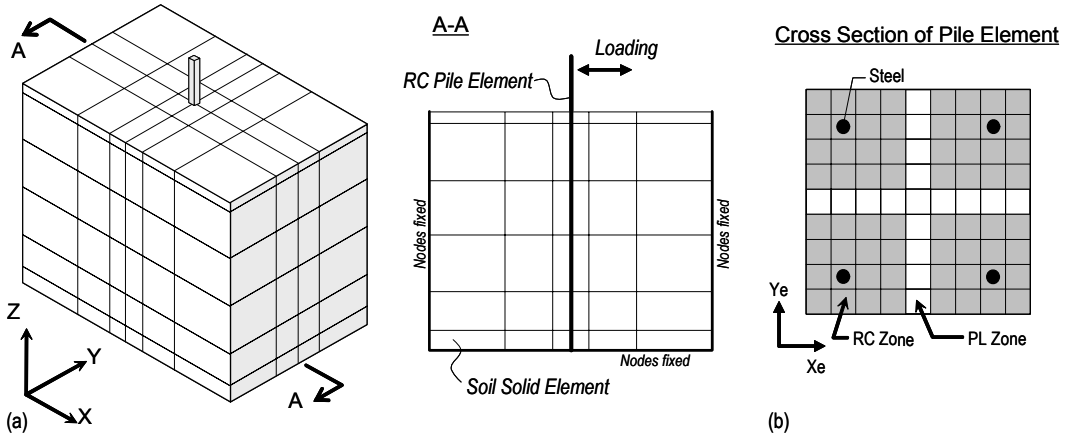

Figure 11. (a) Finite element modeling of pile–soil system; and (b) cross section of pile element.

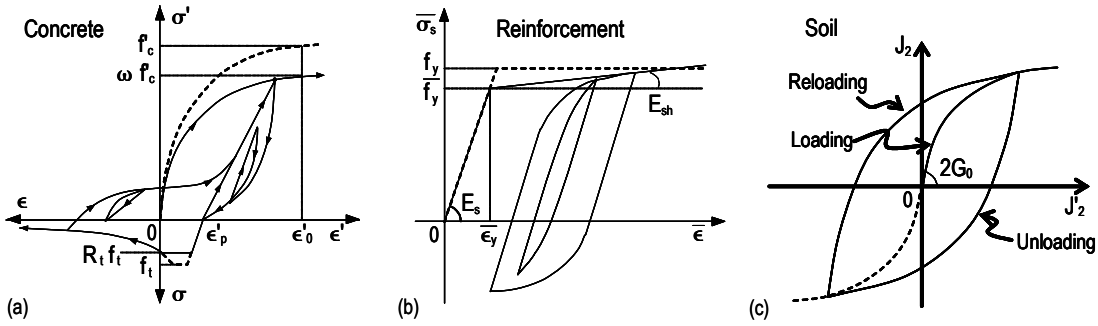

Figure 12. Constitutive laws of: (a) concrete; (b) reinforcement; and (c) soil.

4.2. Analytical results using baseline models

4.2.1. Lateral load and displacement relationships. The hysteresis and skeleton curves of the lateral load and displacement relationships are shown in Figures 13 and 14, respectively. The calculated skeleton curves had a reasonably good agreement with the experimental ones. However, the overestimation of lateral load beyond 50 mm displacement could be observed in both RCR-D and RCC-D. This might have been caused by the high plasticity of the soil near the ground surface, and will be discussed in the next subsection. The lateral load at around the low displacement level in RCC-D was also overestimated. This indicates that the equivalent mesh divisions for square and circular cross sections of the piles are different, i.e. the analytical model with finer mesh divisions may give a more reasonable result for a lateral load of a circular section pile.

Thinner shapes of the inner hysteresis loops could be observed in the analysis relative to the experiment. The variations of the equivalent damping factors calculated from the hysteresis curves are shown in Figure 15. The factors in the analyses were underestimated by about 10% compared with those in the experiments, even in the displacement level in which the piles remained elastic. It seems that the applied soil material model underestimated the energy absorption of the dried soil used in the experiment. Therefore, the damping behaviour of the system should be further investigated for actual soil materials.

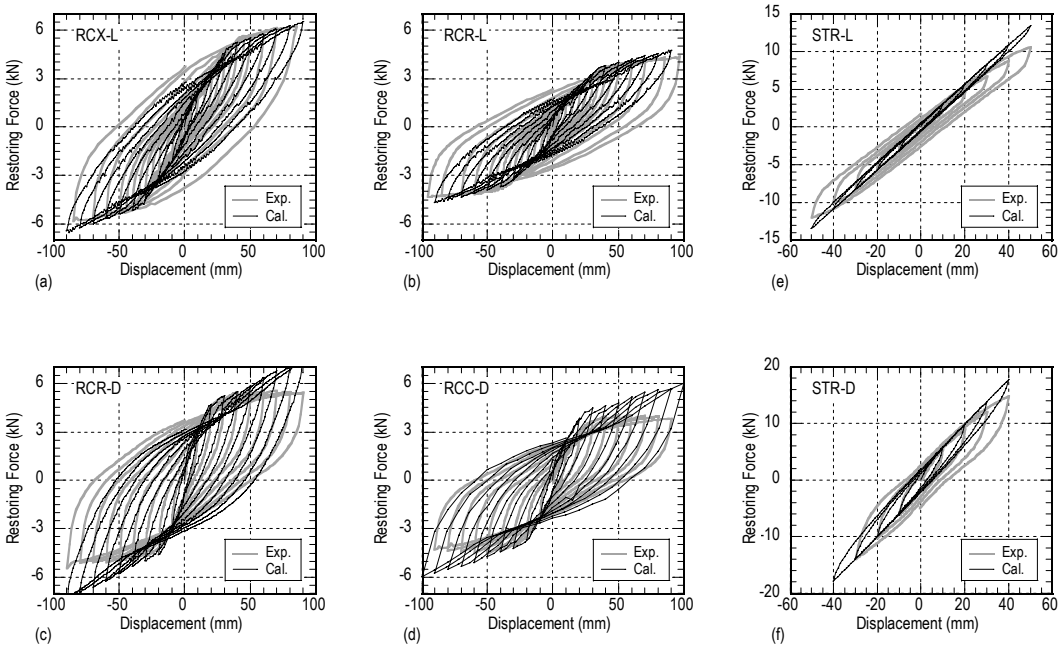

Figure 13. Load–displacement hysteresis curves for all cases.

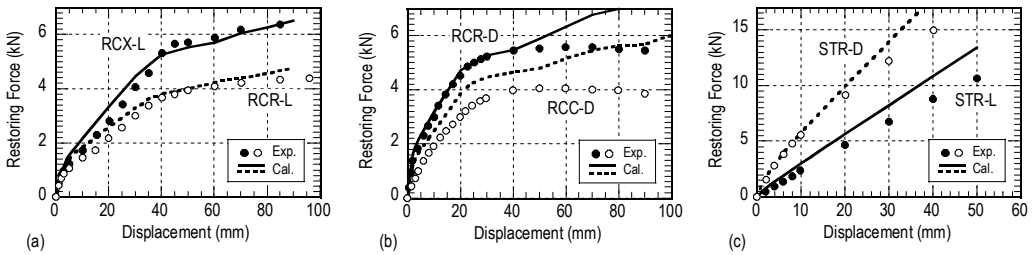

Figure 14. Load–displacement skeleton curves for all cases.

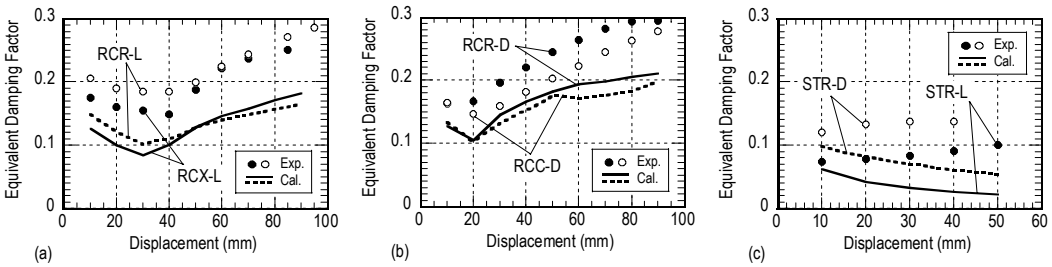

Figure 15. Variations of equivalent damping factors for all cases.

4.2.2. Pile deformation and sectional force distributions. Figure 16 shows the moment, shear force, and curvature distributions along with the experimentally obtained curvature distributions and crack diagram after the loading test for RCR-L. The bold arrow in the crack diagram indicates the location of the widest crack after loading (hereafter, *the maximum damaged depth*). The curvature distributions in the analysis agreed well with the values obtained experimentally. The maximum moment (or no shear force) was observed at GL −0.8 m when yielding of the pile, while at GL −0.5 m in the final stage coincided with the location of the major crack in the crack diagram. Similar results were obtained in the other RC specimens.

The depth at which the shear force was equal to zero (i.e. the location of the maximum moment) was calculated based on linear interpolation, as shown in Figure 17(a), and the results are illustrated in Figure 17(b). The calculated values of the depth in the final stage of loading agreed well with the values obtained experimentally. The location of the maximum moment at the yielding of the pile was farther from the ground surface than that in the final stage of loading. In addition, the distance between these locations was larger in the case in which the pile-to-soil stiffness ratio K_R was relatively high. Chai *et al.* [23] reported that the plastic hinge length in an RC pile was possibly around twice as large as the pile diameter. The analytical results revealed that the plastic hinge length of the pile was dependent on the relative pile-to-soil stiffness as well as on the experienced deformation level.

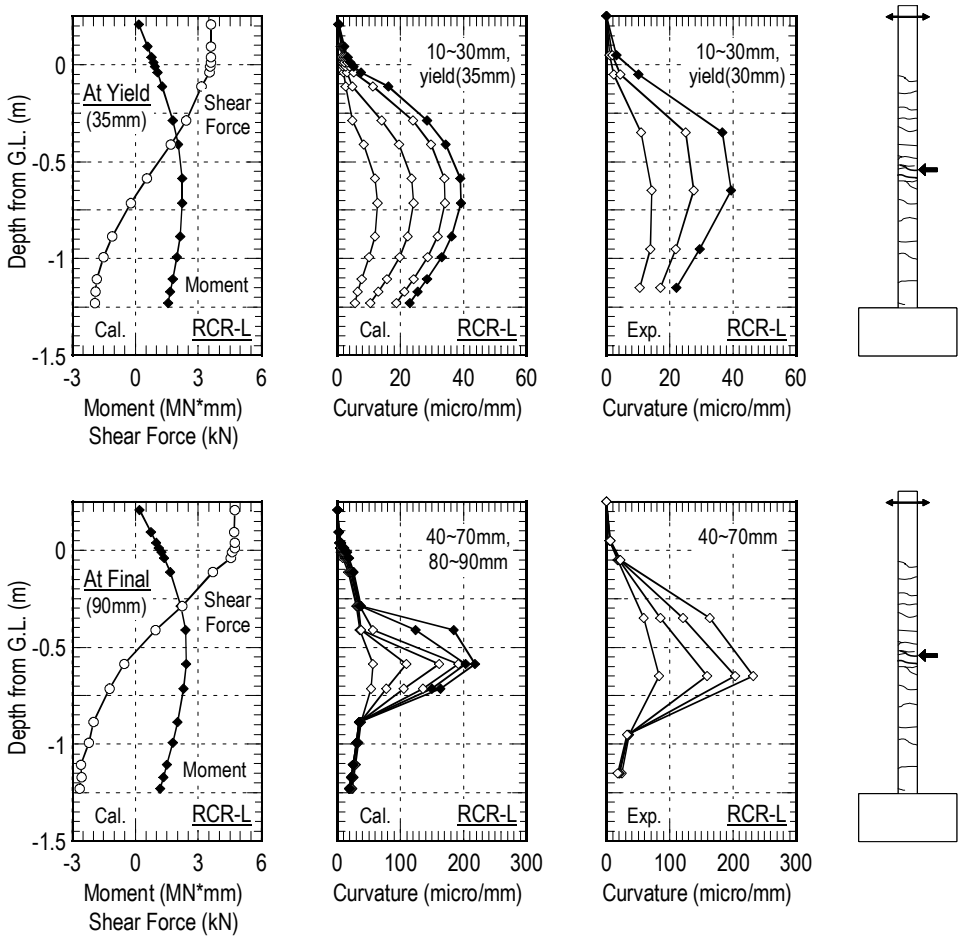

Figure 16. Distributions of moment, shear force, and curvature for RCR-L.

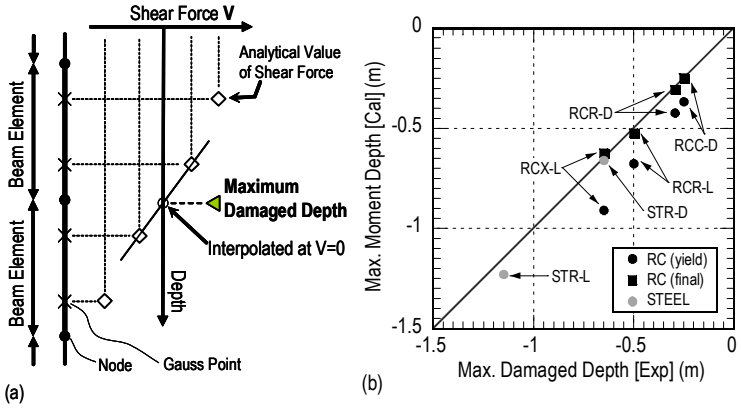

Figure 17. Determination of maximum damaged depth.

4.2.3. Subgrade soil reactions. The measured horizontal soil pressures on the pile surface were compared with the analytically obtained soil reactions. The soil pressures were plotted along with the pile head displacement since it was difficult to obtain the lateral displacement of the pile at each depth using the measured strain data because of the large spacing of the strain gauges. Furthermore, the soil reactions in the analyses were calculated as a secant slope in the shear force diagrams. Figure 18 shows the soil pressure variations for RCR-L, RCR-D, and RCC-D. The measured soil pressure at GL −50mm was eliminated in the figure because it was very low in all the test cases. However, the gradual increase of the pressure at GL −50mm could be observed in the analytical results due to ignorance of the detailed material behaviours of sand in the analysis such as dilatation. The increase resulted in the underestimation of the pressure at GL −650 mm in RCR-L and at GL −350 mm in RCR-D in spite of the similar total soil reactions. In RCC-D, the pressure at GL −350 mm was overestimated from the beginning of loading, which may have resulted in overestimation of the lateral load at the pile head.

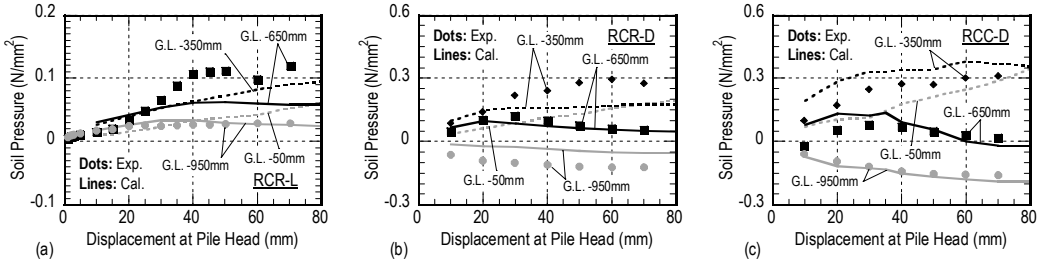

Figure 18. Variations of soil pressures on pile surface for: (a) RCR-L; (b) RCR-D; and (c) RCC-D.

4.2.4. Summary. A beam element model without joint elements between pile and soil was assembled based on single-layer model investigations. These analytical treatments were intended to obtain equivalent soil reactions and, therefore, should be applied only to the DOF-reduced analysis. The investigation proved that the proposed FE model can predict the cyclic behaviour of a laterally loaded single RC pile with reasonable accuracy, in spite of the slight difference of soil pressure distribution and the overestimation of lateral load beyond a certain displacement level. They were both induced by soil strain localization near the ground surface.

4.3. Influence of interfacial behaviour on response of RC piles

The beam element model with joint elements provided a ceiling of subgrade reactions of soil, as previously discussed in Section 3. In spite of the underestimation of the subgrade soil reaction, the grouping of the current soil model and the beam with joint element model might have a possibility of relieving the above-mentioned overestimation of the lateral load beyond the certain displacement level. From this perspective, an attempt was made to apply several types of joint element models in terms of localized interfacial behaviours. A discussion on the modification of the soil material model itself will be reported in the future.

4.3.1. Interfacial behaviours and modeling. The joint element provided at the pile–soil interface was exactly the same as that used in Section 3, as shown in Figure 5. The sectional area of the joint element was defined as the pile width multiplied by the element length. Moreover, the joint elements were arranged in only one direction because the applied load in the targeted experiment was unidirectional. The contact area and the element arrangement for bidirectional problems should be examined in the future.

The influence of the tensile force at the rear surface of the pile has already been discussed. However, the pile–soil cyclic interaction, especially the localized behaviour at the pile–soil interface, is affected by both the initial level of the lateral earth pressure and the sand consolidation caused by the pile's deformation, as illustrated in Figure 19. The four types of linear/non-linear joint models in Figure 20 related to the above-mentioned effects were already examined by the authors in a previous paper [13]. Here, model EL is a perfect elastic model with high normal stiffness, as shown in Figure 20(a). The nodes in the pile and the soil elements, connected by the joint element with model EL, can move with perfect consistency, as they do in the model without joint elements. Model EP is a no-tension model that incorporates the initial lateral earth pressure. Model NT is a simple no-tension model, and Model EPC includes the effect of sand consolidation caused by the pile's cyclic deformation. The previous results concluded that sand consolidation had little influence on pile behaviour. Therefore, the effects of the tensile force and the initial earth pressures were examined using model EL and EP. The shear friction at the interface was completely ignored in this analytical investigation.

In the targeted experiment, the measured initial earth pressure coefficient $K_{h/v}$, which was defined as the ratio of horizontal to vertical pressure, ranged from 0.5 to 0.7 in the cases of loose soil and from 2.3 to 4.0 in the cases of dense soil. In contrast, the initial $K_{h/v}$ in the analysis was around 0.4 because a very simple soil constitutive law independent of the average stress state and a constant value of Poisson's ratio at all possible strain levels were applied. Therefore, in model EP, the stiffness-change point was shifted towards the tension side so that the released stress from the initial earth pressure during pile deformation coincided with that in the experiment, as illustrated in Figure 20(b).

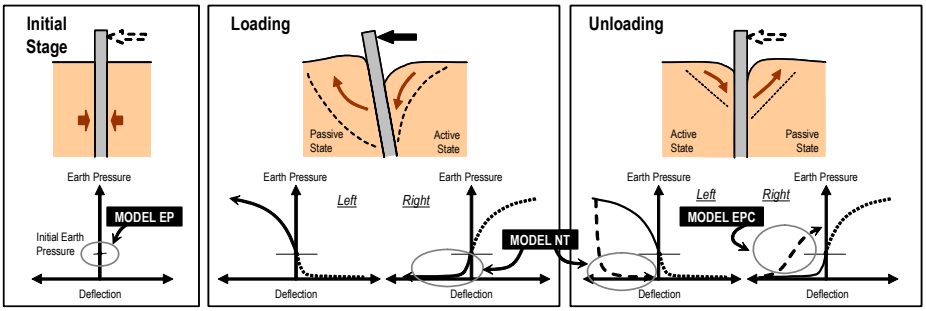

Figure 19. Interfacial behaviour idealization of soil around pile.

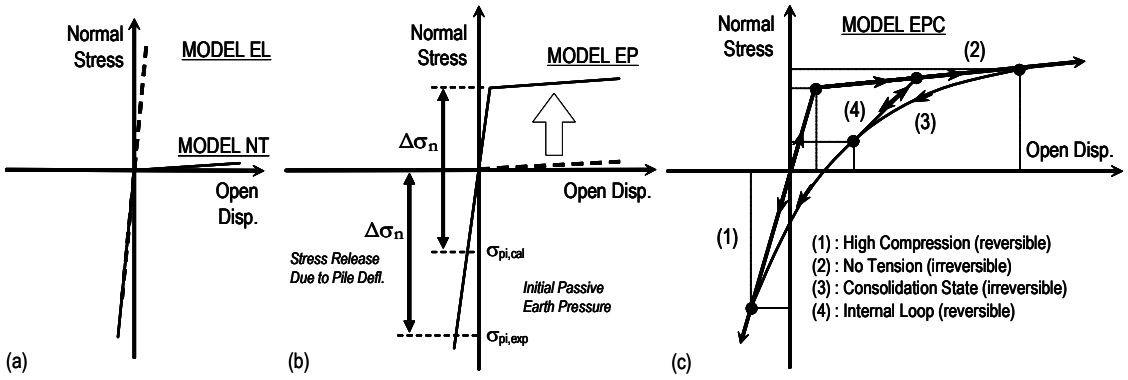

Figure 20. Constitutive laws of joint element: (a) model EL and NT; (b) EP; and (c) EPC.

4.3.2. Influence of interfacial behaviours. The representative skeleton curves of the lateral load and displacement relationships in the RC piles are illustrated in Figure 21. Here, 'NO' indicates the analytical results using the baseline models without the joint elements described in the previous subsection. Slight differences of lateral loads, which originated from the division of soil elements around the pile shown in Figure 5, could be seen between the results of NO and EL. However, these differences are ignored in the discussion here. The hardening in the load–displacement curves, which could be seen in the results for model EL, was relieved in the results for model EP, especially in the cases of RCX-L and RCR-L. This indicates that the hardening in the load–displacement curve in the analysis was induced due to strain hardening in the soil element at the rear of the pile, that is, the effect of the assumption of the tangential shear modulus beyond 1% of shear strain in the applied soil material model. The variations in the equivalent damping factors are shown in Figure 22. The effect of interfacial behaviour on the damping was about 3 and 5% in the cases of loose sand and of dense sand, respectively.

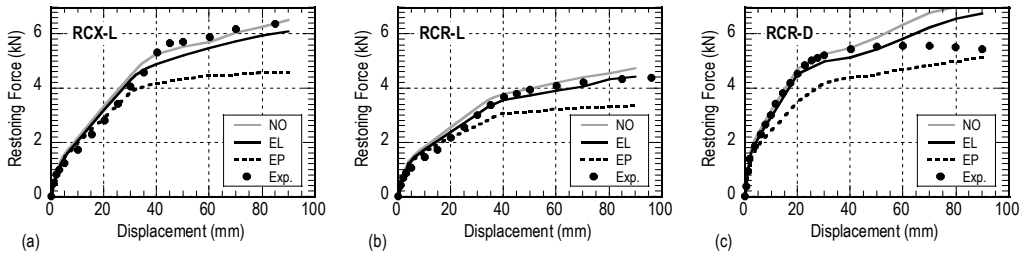

Figure 21. Load–displacement skeleton curves in: (a) RCX-L; (b) RCR-L; and (c) RCR-D.

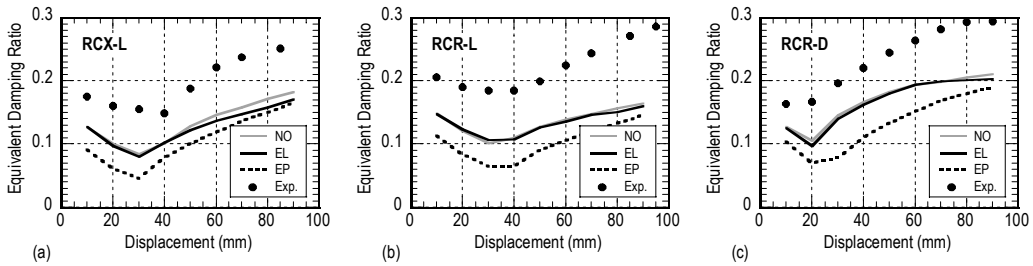

Figure 22. Variations of equivalent damping factors in: (a) RCX-L; (b) RCR-L; and (c) RCR-D.

Figure 23(a) shows the maximum damaged depth of a pile in the analyses compared with those in the experiments. All the values of the depths were plotted with the relative pile-to-soil stiffness K_R in Figure 23(b). The tendency observed in the experiment that the maximum damaged depth became large in the case of high relative pile-to-soil stiffness could also be seen in the analytical results. However, in model EP, the depth was overestimated by about 40–50% of the actual depth resulting in an underestimation of the lateral load based on the mechanism of force transmission between the pile and the soil, as already reported in a previous paper [24].

From the discussion above, it can be concluded that the use of joint elements having no tensile stiffness could relieve hardening in the lateral load–displacement relationships due to the definition of the shear modulus at a large strain level in the applied soil material model. However, the lateral load itself and the damping of the system were relatively underestimated. This might have been caused by the overestimation of the maximum damaged depth.

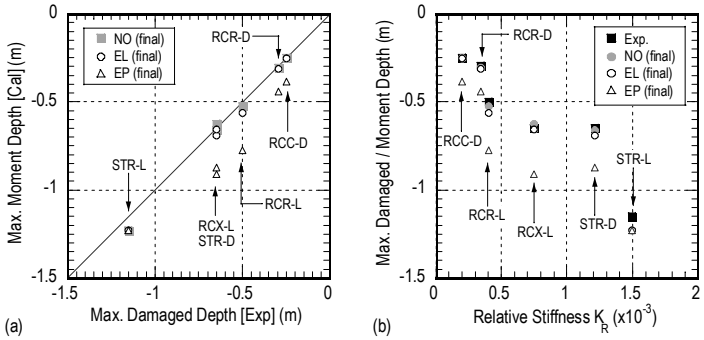

Figure 23. Variations of maximum damaged depth at final stage of loading.

5. CONCLUSIONS

In order to evaluate the overall response of a structural system including its foundation and surrounding soil, response analysis in time-domain using FEM, in which seismic motion is input to the engineering base layer, is an advanced technique that can automatically and explicitly consider soil–structure interactions. However, particularly in the case of a structure supported by a large number of piles, it is still difficult to model all of the members using full 3-D solid elements because of the large number of degrees of freedom in such an analytical model. Thus, a simpler alternative model is still needed in order to reduce analytical costs. The principal objective of this paper is to propose an equivalent DOF-reduced model for pile–soil interaction analysis that can provide a reasonable analytical result with reasonable analytical costs.

At first, the influence of pile modeling on the resultant subgrade soil reaction was investigated based on single-layer FE models, and an equivalent DOF-reduced model using a beam element was proposed. In the model, the grouping of the following analytical conditions was suggested: (1) simple hyperbolic-type soil shear model with the occurrence of principal tensile stress, (2) no joint element between pile and soil, (3) relatively coarse mesh division around pile (in this paper, about three times pile diameter), (4) a low order of Gauss integration scheme in soil elements to avoid stress localization (2 in this paper).

The cyclic behaviour of a laterally loaded single RC pile was then simulated by using the proposed DOF-reduced model. The analytical results were fully compared with the experimental results, and the proposed equivalent model was verified based on the load and displacement

relationships, deformation of the pile, and soil pressures on the pile surface. The proposed model can predict the cyclic behaviour of a laterally loaded single RC pile with reasonable accuracy, in spite of slight differences in soil pressure distribution and the overestimation of lateral load beyond a certain displacement level. Also investigated was the effect of interfacial characteristics between pile and soil on the behaviour of a laterally loaded pile. The use of joint elements having no tensile stiffness could relieve the hardening in lateral load–displacement relationships. However, the lateral load itself and the damping of the system were underestimated. Hence, it was concluded that the proposed model without any joint elements was relatively better to use for a single RC pile–soil system.

In the application of the proposed model to actual structures, measurement error and the accuracy of soil parameters as well as the adequacy of the applied soil constitutive model should be fully examined. Furthermore, in the future, for its application to the response analysis of an overall structural system including pile–soil interaction, the analytical model must be carefully verified in terms of three-dimensional behaviour such as group-pile effect.

ACKNOWLEDGEMENTS

The authors wish to gratefully acknowledge the cooperation of Prof. F. Tatsuoka, Prof. K. Konagai, Assoc. Prof. M. Abe, and Assoc. Prof. X. An of The University of Tokyo, and Prof. A. Machida of Saitama University, as well as the cooperation of the members of the Structural Material Laboratory of Saitama University.

REFERENCES

1. JSCE Committee of Civil Engineering of Nuclear Power Facilities. *Seismic Design Manual for Nuclear Electric Power Facilities*. JSCE: Tokyo, Japan, 2005 (in Japanese).
2. Japan Society of Civil Engineers. Standard Specifications for Concrete Structures—2002: Seismic Performance Verification. *JSCE Guidelines for Concrete No. 5*, 2005.
3. Chang YL. Discussion on “lateral pile loading tests” by Feagin. *Transactions of the ASCE* 1937; **102**:272–278.
4. Broms BB. Lateral resistance of piles in cohesionless soils. *Journal of the Soil Mechanics and Foundation Division* (ASCE) 1964; **90**(SM3):123–156.
5. Poulus HG. Laterally load–deflection prediction for pile groups. *Journal of Geotechnical Engineering* (ASCE) 1975; **101**(GT1):19–34.
6. Koda M, Takemura J, Kusakabe O. Modelling and evaluation of *P–Y* curves of single pile in sand. *Journal of Structural Mechanics and Earthquake Engineering* (JSCE) 2000; **645**(50):191–207 (in Japanese).
7. Randolph MF. The response of flexible piles to lateral loading. *Geotechnique* 1981; **31**(2):247–259.
8. Muqutadir A, Desai CS. Three-dimensional analysis of a pile-group foundation. *International Journal of Numerical and Analytical Methods in Geomechanics* 1986; **10**:41–58.
9. Trochanis AM. Three dimensional nonlinear study of piles. *Journal of Geotechnical Engineering* (ASCE) 1991; **117**(3):429 –448.
10. Wakai A, Gose S, Ugai K. 3-D elasto-plastic finite element analyses of pile foundations subjected to lateral loading. *Soils and Foundations* 1999; **39**(1):97–111.
11. Zhang F, Kimura M, Nakai T, Hoshikawa T. Mechanical behavior of pile foundations subjected to cyclic lateral loading up to the ultimate state. *Soils and Foundations* 2000; **40**(5):1–17.
12. Maki T, Mutsuyoshi H, Maekawa K. Applicability of fiber model to RC pile–soil interaction analysis.

Journal of Materials, *Concrete Structures and Pavements* (JSCE) 2003; **746**(61):57–70 (in Japanese).
13. Maki T, Mutsuyoshi H. Restoring force and deformation of reinforced concrete piles. *Journal of Materials*, *Concrete Structures and Pavements* (JSCE) 2001; **683**(52):103–118 (in Japanese).
14. Maki T, Mutsuyoshi H. Effect of local characteristics between pile and soil on seismic behavior of RC piles under ground. *fib 2003 Symposium on Concrete Structures in Seismic Regions* (Proceedings in CD form), Athens, Greece, 2003; paper No.140.
15. Maki T, Mutsuyoshi H. Seismic behavior of reinforced concrete piles under ground. *Journal of Advanced Concrete Technology* (JCI) 2004; **2**(1):37–47.
16. Ishida T *et al.* Static and dynamic mechanical properties of materials for model tests (Gifu sand) under low confining stress. *Research Report of Electrical Power Center Research Institute*, *No. 380045*, 1981; 1–36 (in Japanese).
17. Poulos HG. Behavior of laterally loaded piles: I—single piles. *Journal of the Soil Mechanics and Foundations Division. Proceedings of ASCE* 1971; **97**(5):711–731.
18. Maki T, Maekawa K, Mutsuyoshi H. Effect of pile modeling on behavior of RC piles under ground. *Proceedings of the Japan Concrete Institute* 2004; **26**(2):1165–1170 (in Japanese).
19. Okamura H, Maekawa K. *Nonlinear Analysis and Constitutive Models of Reinforced Concrete.* Gihodo Shuppan: Tokyo, Japan, 1991.
20. Maekawa K, Pimanmas A, Okamura H. *Nonlinear Mechanics of Reinforced Concrete*. Spon Press: London, U.K., 2003.
21. Ohsaki Y. Some notes on Masing's law and non-linear response of soil deposits. *Journal of the Faculty of Engineering*, *The University of Tokyo* (*B*) 1980; **35**(4):513 –536.
22. An X, Maekawa K, Okamura H. Numerical simulation of size effect in shear strength of RC beams. *Journal of Materials*, *Concrete Structures and Pavements* (JSCE) 1997; **564**(V-35):297–316.
23. Chai YH, Hutchinson TC. Flexural strength and ductility of extended pile-shafts—II: experimental study. *Journal of Structural Engineering* (ASCE) 2002; **128**(5):595 –602.
24. Maki T, Mutsuyoshi H. Study on seismic performance of reinforced concrete piles under ground. *Proceedings of the 3rd International Workshop on Performance-Based Seismic Design and Retrofit of Transportation Facilities*, Tokyo Institute of Technology, 2002; 67–78.